IEEE Robotics and Automation Letters (RAL) paper presented at the
2020 IEEE/RSJ International Conference on Intelligent Robots and Systems (IROS)
October 25-29, 2020, Las Vegas, NV, USA (Virtual)

Online Acquisition of Close-Range Proximity Sensor Models for Precise Object Grasping and Verification

Shun Hasegawa, Naoya Yamaguchi, Kei Okada, and Masayuki Inaba

***Abstract*— This study presents an approach for acquiring model parameters of close-range approximate proximity sensors on a robot hand using long-range distance sensors while that hand is grasping an object. The acquired models are used to generate a precise close-range distance output. We aim herein to acquire proximity sensors that have little dependence on object properties and that can sense a wide range (i.e., both close and long ranges). Simple close-range sensors strongly depend on object properties such as reflectance, material, volume, and/or conductivity, whereas long-range sensors cannot precisely measure the close range. To accomplish our goal, we fused close- and long-range sensors. Simple fusion remains object dependent at the close range. Hence, we acquired an object-dependent parameter in the close-range sensor model using the distance output of the long-range sensor at the overlap of the two sensor types. Through real robot experiments, we evaluated the precision of the generated distance output at the close range and found it useful to the precise grasping of compliant objects. We also confirmed that the acquired object-dependent parameter can verify ultra-thin object grasping.**

I. INTRODUCTION

This study presents an approach for acquiring the model parameters of close-range approximate proximity sensors on a robot hand using long-range distance sensors while that hand is grasping an object (Fig. 1). Each model denotes the relationship of the sensor output and distance to the sensed object. Proximity sensor modules composed of both close- and long-range sensors (Fig. 2) are created and utilized herein to realize the acquisition. This study also shows the model application to the precise grasping of compliant objects and verification of ultra-thin object grasping.

Proximity sensors mounted on robot hands have been utilized in many studies on robotic grasping [1]–[13]. We believe that these sensors can extend tactile information, seamlessly connect it with visual information, and realize continuous sensing in robotic manipulation. Accordingly, several types of proximity sensors have been used for robotic grasping including optical reflection intensity sensors [1, 3]–[5, 8, 10, 13], capacitive sensors [2, 7], sound sensors [6], optical sensors using multiple modulated light sources [9], and optical time-of-flight (ToF) sensors [11, 12]. Table I describes the relationships between these sensors. The first two types of sensors, which are optical reflection intensity and capacitive sensors, can sense a close range ($< 10\,\mathrm{mm}$), but strongly depend on object properties such as reflectance, material, volume, and/or conductivity. In addition, the maximum measurable distances of these close-range approximate sensors are short. Sound and optical sensors using multiple modulated light sources mostly overcome dependence on object properties, but their measurable distances are still short (i.e., sound sensors: $3\,\mathrm{mm}$; optical sensors: $20\,\mathrm{mm}$). Optical ToF sensors have little dependence on the object properties and can measure a long distance, but cannot precisely measure a close range. This drawback causes a thick fingertip to prevent objects from entering the dead zone of these long-range distance sensors. In summary, no sensor that exhibits little dependence on the object properties and can sense a wide range (i.e., both close and long ranges) has

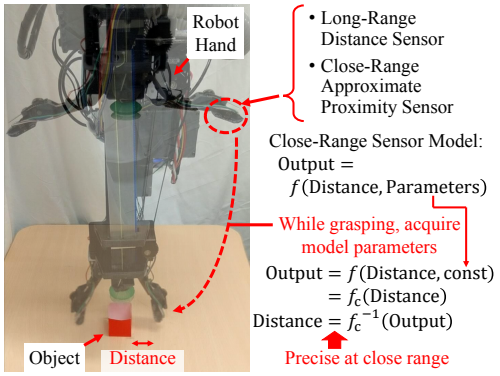

Fig. 1. Illustration of the online acquisition of close-range proximity sensor models. Our system acquired the model parameters of the close-range approximate proximity sensors on the robot hand while that hand was grasping an object. Using the acquired models, our system calculated the output representing the distance to the object precisely at close range.

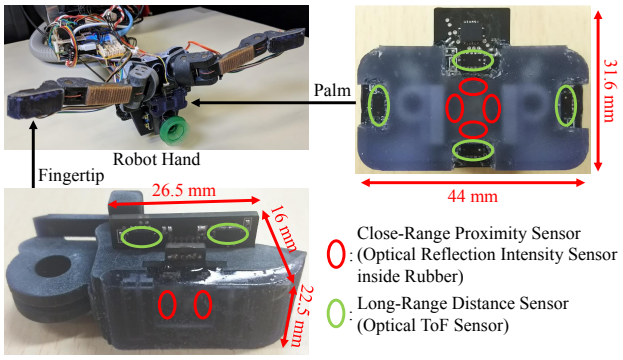

Fig. 2. Proximity sensor modules with close- and long-range sensors. The fingertip and palm modules were made for the previously developed robot hand [10]. Our modules were compact enough to keep the sizes of the fingertips and the palm even though each module had multiple points of precise close-range measurement.

S. Hasegawa, N. Yamaguchi, K. Okada, and M. Inaba are with JSK Laboratory, Graduate School of Information Science and Technology, The University of Tokyo, 7-3-1 Hongo, Bunkyo-ku, Tokyo 113-8656, Japan hasegawa@jsk.imi.i.u-tokyo.ac.jp

TABLE I
RELATIONSHIPS BETWEEN THE PROXIMITY SENSORS USED FOR ROBOTIC GRASPING. THIS STUDY AIMS TO CREATE A SENSING SYSTEM THAT HAS LITTLE DEPENDENCE ON THE OBJECT PROPERTIES AND THAT CAN SENSE A WIDE RANGE.

	Optical Reflection Intensity, Capacitive	Optical ToF	Sound [6], With Modulated Light [9]
Close-Range	✓	×	✓
Long-Range	×	✓	×
Little Dependent on Object Properties	×	✓	✓
		This Study (Fusion)	

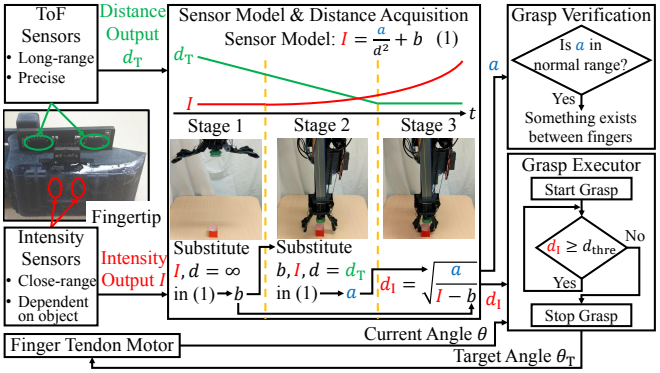

Fig. 3. Overview of the sensor model acquisition, grasping, and verification.

yet been developed.

One of the simplest approaches for features to coexist is to fuse multiple sensors. In this work, we found that fusing a close-range approximate sensor and a long-range distance sensor can accomplish these features even though the fusion seemingly remains dependent on the object properties at a close range. The key to overcoming this dependence is to acquire an object-dependent parameter of the close-range sensor when a sensed object is in the overlapping measurable range of the two sensor types. A sensor model using that parameter then generates a precise distance value to the object from a close-range sensor output. This value remains precise at the close range, where the long-range sensor measurement is not precise. This acquisition is one-shot and can be conducted online while the object is grasped. This feature enables our robot system to adapt to the latest environment. Although some previous studies addressed the object dependence of the close-range approximate sensor [3, 13, 14], their methods were not one-shot and cannot be conducted online. Our sensor modules are compact because only the simple close-range sensor is required to be combined with the long-range sensor.

Moreover, we present herein the application of the acquired sensor models to the precise grasping of compliant objects and verification of grasping ultra-thin objects (i.e., sheets of paper). Fig. 3 depicts the sensor model acquisition, grasping, and verification processes. In grasping compliant objects, when the distance values generated from the fingertip close-range sensors fall below a heuristic threshold, the robot hand stops its fingers to pick up the objects without damaging them by squeezing. The generated values are precise (i.e., little dependence on the object properties). Hence, the threshold becomes common to objects with different properties. We chose the picking-up motion for our module application because allowing a non-damaging grasp of compliant (fragile) objects is considered as one of the advantages of proximity sensors [6, 9]. The reaction force from these objects tends to be too small for general pressure sensors to detect, and these pressure sensors probably cannot stop the fingers before the objects are crushed.

To verify the grasping of ultra-thin objects, our system detects whether a sheet exists between the fingers using the object-dependent parameters of the fingertip close-range sensors acquired online. Each sensor senses an opposed fingertip if nothing exists between the fingers. In this case, the acquired parameters should be much different from those in the case when sensing paper because we use optical sensors, and our fingertips are covered with transparent rubber based on our previous work [10, 13]. By contrast, conventional grasp detection methods using tactile information [15]–[19] face difficulty in distinguishing an ultra-thin object from nothing because the fingertip deformation and the opening width between the fingertips are almost the same between the two cases because of the great compatibility of the object with the fingertips and the object thinness.

In summary, the main contributions of this paper are as follows:

- online parameter acquisition in a model of a close-range approximate proximity sensor, especially an object-dependent parameter, using overlap with a long-range distance sensor (§II-A and §II-B);
- precise measurement of wide-range distances (precision also means little dependence on sensed object properties) using the acquired models (§II-B);
- composition of proximity sensor modules with two sensor types to verify the abovementioned principles (§III and §IV); and
- application of the obtained precise distance values and object-dependent parameters to the grasping of compliant objects and verification of ultra-thin object grasping (§II-C and §IV).

II. ONLINE SENSOR MODEL ACQUISITION AND PRECISE GRASPING WITH VERIFICATION

A. Model of Close-range Sensors

As with our previous studies [10, 13], we used an optical reflection intensity sensor as the close-range sensor and embedded it in transparent rubber. We assumed the following sensor model on the basis of the inverse-square law of light [13]:

$$I = \frac{a}{d^2} + b \tag{1}$$

where I [digit] is the intensity sensor output, d [mm] is the distance to the sensed object, a [digit $\cdot$ mm^2] is the object-dependent parameter, and b [digit] is the offset parameter mainly caused by the light reflection in the rubber. Note

that I is expressed as a digital value (digit) from the A/D converter in the sensor. The former parameter was mainly influenced by the object reflectance and the optical loss in the rubber. The rubber state (e.g., bubble density and surface smoothness) in front of each sensor differed. Thus, the parameters also differed from sensor to sensor. Equation (1) is simple; hence, its calculation is in real time.

B. Online Model Acquisition and Distance Measurement

When grasping an object, a robot hand may first be far from the object and then approach it. In this process, we first acquired the offset parameter b as the intensity output I when the object was too far for the intensity sensor to sense ($d = \infty$ in (1)). Subsequently, we acquired the object-dependent parameter a when the object was sensed by both the intensity sensor and the long-range distance sensor (i.e., optical ToF sensor). This was conducted by substituting the ToF sensor output d_{T} [mm] for d in (1). As a result, our grasping motion can be divided into the following three stages:

1) the object is far, and only the ToF sensor detects it;
2) both the ToF and intensity sensors detect the object; and
3) the object is too close for the ToF sensor to detect precisely, and the intensity sensor detects it.

Fig. 3 illustrates the three stages and the overview of the sensor model acquisition.

We can acquire a using I, b, d_{T}, and (1) if the ToF and intensity sensors are directed to the same direction and close enough such that d_{T} is equal to d (i.e., distance from the intensity sensor to the sensed object). This fact can be extended to the case in which two sensors are on different parallel planes, whose height difference d_{o} [mm] is known, by redefining d_{T} as the distance shorter than the original ToF output by d_{o}. We used this extended fact to acquire a. In addition, although I sometimes becomes bigger than b even at Stage 1 and a can be calculated, we set $a = 0$ in that stage because a calculated with very small $I - b$ is small and unreliable. Consequently, a can be calculated as follows:

$$a = \begin{cases} 0 & (\text{Stage 1}) \\ (I-b){d_{\mathrm{T}}}^2 & (\text{Stage 2}) \end{cases} \tag{2}$$

The calculation for Stage 2 is conducted any time I and d_{T} have almost the same timestamp and the heuristic condition of Stage 2, which depends on sensor selection and placement, is satisfied.

In Stages 2 and 3, the latest a and (1) are used to calculate the precise distance value d_{I} [mm] from the intensity output. The equation is explicitly written as follows:

$$d_{\mathrm{I}} = \begin{cases} \infty & (\text{Stage 1}) \\ \sqrt{\frac{a}{I-b}} & (\text{Stages 2 and 3}) \end{cases} \tag{3}$$

C. Precise Grasping with Verification

Precise grasping was conducted with d_{I} (i.e., distance value generated from the intensity output) from the fingertips to prevent our robot hand from squeezing the compliant objects. Fig. 3 describes the flow. First, the robot commands the finger tendon motor to rotate up to the target angle θ_{T} [rad]. With this command, two underactuated fingers of the hand start closing. While the motor is pulling the tendon ($\theta < \theta_{\mathrm{T}}$), the robot continuously checks whether each d_{I} from the fingertips becomes under the heuristic threshold d_{thre} [mm]. When every d_{I} becomes under d_{thre} ($d_{\mathrm{I}} < d_{\mathrm{thre}}$) (i.e., both of the fingertips are appropriately close to the target object), the robot commands the motor to stop ($\theta_{\mathrm{T}} = \theta$). After a delay between the stop command and a stop of the fingers, the fingertips touch the object gently enough to avoid squeezing, but firmly enough to pick it up. Owing to the precision of d_{I}, d_{thre} becomes common to objects with different reflectance values.

After grasping, the robot verifies whether something exists in the hand using a (i.e., the object-dependent parameter of the intensity sensor) from the fingertips. The object existence is detected if every a is in a heuristic range. Although a differs from sensor to sensor as mentioned in §II-A, we could use one range for the sensors used in the experiments (§IV).

III. PROXIMITY SENSOR MODULE WITH CLOSE-RANGE AND LONG-RANGE SENSORS

This section describes the implementation of the proximity sensor modules with both close- and long-range sensors created for the precise measurement of wide-range distances. We used an optical reflection intensity sensor as the close-range sensor and an optical ToF sensor as the long-range sensor. Our module was compact (fingertip module: $22.5\,\mathrm{mm} \times 26.5\,\mathrm{mm} \times 16\,\mathrm{mm}$, Fig. 2) and had a wide range (at least 5–400 mm).

A. Sensor Selection

As with our previous studies [10, 13], we used VCNL4040 (VCNL4040M3OE, Vishay Semiconductors) as the optical reflection intensity sensor. In our usage, where the sensor was embedded in transparent rubber and its LED current was 180 mA, the range was approximately 5–60 mm. This value was similar to the range of approximately 0.5–7 cm, which was shown in the previous study, using a sensor from the same family (i.e., VCNL4010) with a similar configuration (i.e., embedded in transparent rubber with 120 mA LED current) [8]. By contrast, the range was narrower than that in the VCNL4040 catalog [20] (0–200 mm) probably because the rubber added an error to the measurement [8] and the catalog range was a combined result of multiple current settings. To acquire the sensor parameters, the ToF sensor range should have a sufficient overlap with the intensity sensor because the acquisition requires the valid simultaneous values of both the intensity and ToF sensors. In addition, a longer maximum measurable distance is preferred for the ToF sensor. Tininess is also required for the sensor. Therefore, we used VL53L0X from STMicroelectronics as the ToF sensor. The carrier board seller [21] and the catalog of that sensor [22] indicate a size of $4.4\,\mathrm{mm} \times 2.4\,\mathrm{mm} \times 1.0\,\mathrm{mm}$ and a range of at least 30–400 mm. Practically, we considered the minimum distance as 45 mm to use the sensor against various objects. The minimum measurable distance of VL53L1X, which

was in the same sensor family as VL53L0X, was $40\,\mathrm{mm}$ according to its catalog [23]. This minimum distance was too long considering that a practical minimum distance seems longer than a catalog value. Although VL6180X was also in the same family, its maximum measurable distance was $100\,\mathrm{mm}$ [24], and VL53L0X was more preferred.

As for the accuracy of VL53L0X according to its catalog [22], the standard deviation of the measured distance was 5% when the timing budget of VL53L0X was $20\,\mathrm{ms}$ (high-speed range profile), which was used herein. This deviation was included in the deviation of d_I through (2) and (3), indicating that the standard deviation of d_I should be more than 5%. What increases that deviation from 5% should be the standard deviation of VCNL4040, which was not described in its catalog [20].

B. Fingertips and Palm Including Our Sensor Modules

We integrated our sensor modules into the fingertips and the palm of the robot hand proposed in our previous work [10]. The fingers of the robot hand were developed from the Yale OpenHand Project [25]. As with our previous work, the intensity sensors were implanted in non-slip rubber on the fingertips. Although the previous work used a transparent silicon elastomer (Sylgard 184 from Dow Corning) as the rubber, we used herein a transparent urethane resin (GUMMY CAST Transparence from NISSIN RESIN) to increase friction and avoid cure inhibition from occurring when the silicone was cured in a mold printed with an ultraviolet three-dimensional printer [26].

Although we also tried to embed the ToF sensor in the rubber, we found that the sensor always outputs approximately $20\,\mathrm{mm}$. We think that this is mainly caused by the small bubbles in the rubber. However, we cannot conduct sufficient degassing because the pot life of the rubber was short (less than $10\,\mathrm{min}$). Therefore, two solutions were implemented for the ToF sensors:

1) protrusions on the side of the rubber were installed to place the sensors, and
2) the rubber area was reduced, and cavities were created to place the sensors.

For the fingertips, we selected solution 1 to maintain the friction for a stable object manipulation. For the palm, we selected solution 2 because the palm was originally large, and reduction only had minimal influence.

Fig. 4 shows the fingertip with its manufacturing process. Two PCBs were used for each fingertip. One had two intensity sensors and was embedded in the rubber. The other was mounted on the back of the fingertip with a screw and had a protrusion from the fingertip containing two ToF sensors. Mounting on the back widened the overlap between the intensity and ToF sensor ranges by $6\,\mathrm{mm}$ (i.e., $d_\mathrm{o} = 6\,\mathrm{mm}$, using d_o introduced in §II-B). This was good for the sensor model acquisition, as stated in §III-A. The PCBs were connected via polyurethane enamel wires. The intensity and ToF sensors had $\mathrm{I}^2\mathrm{C}$ interfaces and different slave addresses. Hence, we prepared two $\mathrm{I}^2\mathrm{C}$ lines per fingertip, and each line had one intensity sensor and one ToF sensor. As a result, six

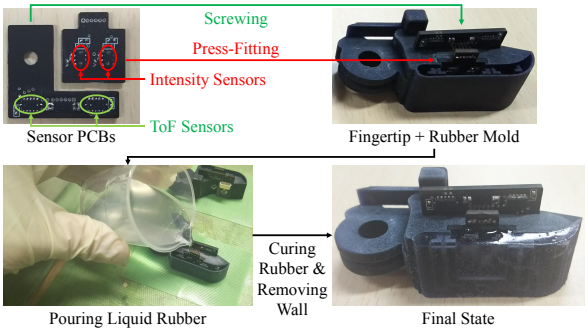

Fig. 4. Manufacturing process of the fingertip. The fingertip had a PCB with two intensity sensors and a PCB with two ToF sensors. The PCBs were press-fitted or screwed to the fingertip, which additionally serves as a rubber mold.

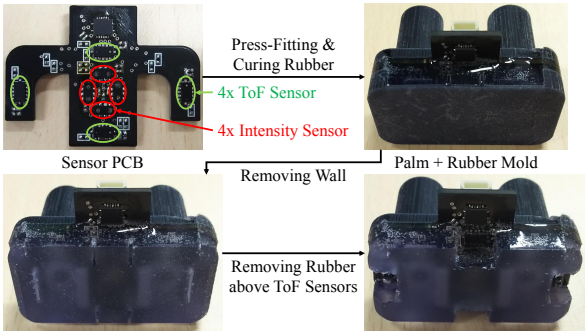

Fig. 5. Manufacturing process of the palm. The palm had a PCB with four intensity sensors and four ToF sensors. The PCB was press-fitted to the palm, which additionally serves as a rubber mold. After rubber curing and mold wall removal, the rubber region above each ToF sensor was removed such that the sensor can precisely measure the distance.

wires came from each fingertip and were connected to a computer (UP Board from AAEON) in the robot hand.

Fig. 5 shows the palm with its manufacturing process. The used PCB included four intensity sensors around its center and four ToF sensors near its outer edge. As a result, $d_\mathrm{o} = 0\,\mathrm{mm}$ using d_o introduced in §II-B. After rubber curing on the PCB, we removed the rubber region above each ToF sensor by deepening the cracks made by the mold using a box cutter and a screwdriver. The rubber remaining in the depressions of the light emitter and light collector in each ToF sensor must be removed with a marking pin; otherwise, the measurement will be incorrect. The palm PCB had an $\mathrm{I}^2\mathrm{C}$ multiplexer (PCA9546A, Texas Instruments), and all sensors were connected to that multiplexer. Consequently, four wires came from the palm and were connected to the computer.

C. Obtainment of Sensor Outputs

We applied the following low-pass filter after obtaining raw ToF and intensity sensor values at $20\,\mathrm{Hz}$:

$$F[T] = 0.3f[T] + 0.7F[T-1] \tag{4}$$

where T is the current time step, $f[T]$ is the current raw sensor value, and $F[T-1]$ is the output of the low-pass filter on the previous time step.

As explained in §II-B, we applied the offset d_o to the

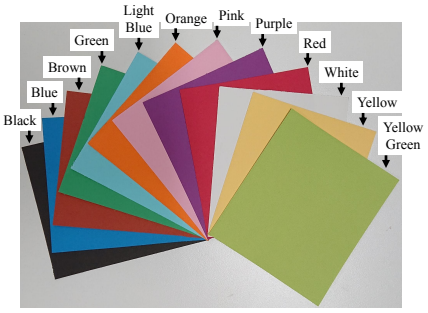

Fig. 6. Sheets of paper used in distance measurement (§IV-A) and verification of ultra-thin object grasping (§IV-C). All 12 sheets had different colors. Each had the same color on both sides and 0.19 mm thickness.

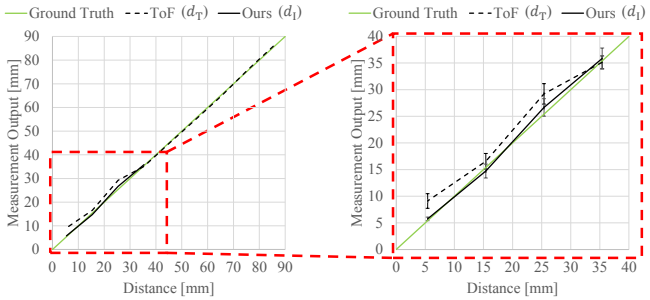

Fig. 7. Distance output of our sensor module. The solid black line shows the distance output generated from the intensity sensor (d_I). The broken black line shows the ToF sensor output (d_T). These lines were created with linear interpolation between the means of 120 measurements (10×12 colors). The green line shows the ground-truth values (ideal for the sensors). The right graph is an enlarged view of the left graph. Each error bar in the right graph represents one standard deviation of 120 measurements. The line of d_I is close to the ground-truth line, and the line of d_T shifts upward at a distance ≤ 25.4 mm. The error bar of d_I is very small at 5.4 mm.

filtered value of the ToF sensor as follows:

$$d_T = d_{\text{filtered}} - d_o \tag{5}$$

where d_{filtered} is the filtered value. d_o is 6 and 0 mm for the fingertip and palm sensors, respectively, as mentioned in §III-B. The calculated d_T was used for the model acquisition of the closest intensity sensor.

IV. EXPERIMENTS

First, we quantified the precision of the distance measurement by our sensor module and validated that our module was more precise than the measurement using only the ToF sensor (§IV-A). Second, we confirmed that our precise grasping system can suppress the deformation of compliant objects compared to grasping only with the intensity sensors and grasping with the pressure sensors (§IV-B). Third, we validated that our grasp verification system works against colorful ultra-thin objects (§IV-C). Finally, we confirmed that our proposed methods can be applied to picking up and placing ultra-thin objects with recovery from disturbances caused by a person (§IV-D).

In §IV-A and IV-C, we used 12 colored sheets of paper with both sides having the same color (Fig. 6) and with thicknesses of 0.19 mm. In all of the experiments, we defined Stage 2 described in §II-B as when $20\,\text{digit} \leq I - b \leq 1000\,\text{digit}$ and $45\,\text{mm} - d_o \leq d_T \leq 60\,\text{mm}$ are valid. We set the admissible timestamp difference between I and d_T used in (2) to 0.02 s, the threshold of our precise grasping (d_{thre}) to 25 mm, and the range of our grasp verification to $10000\,\text{digit}\cdot\text{mm}^2 \leq a \leq 2000000\,\text{digit}\cdot\text{mm}^2$. In addition, we used one ToF sensor and one intensity sensor, which were the closest to the tip of every finger of our robot hand.

A. Distance Measurement

We conducted 10 measurements of one fingertip sensor module at each of the nine distances against the 12 colored sheets (Fig. 6). The distance between the intensity sensor in the fingertip and the rubber surface was 5.4 mm. Hence, we set this distance as the minimum of the target distances. We also set the measurement step as 10 mm. Thus, the maximum target distance was 85.4 mm. To set the minimum I (intensity sensor output) as b (offset parameter), we first moved the hand 285.4 mm away from the sheet and obtained

TABLE II
TABLE OF DISTANCE OUTPUT OF OUR SENSOR MODULE. THE MEAN, STD, AND E_{max} REPRESENT THE MEAN, STANDARD DEVIATION, AND MAXIMUM ABSOLUTE ERROR OF 120 MEASUREMENTS, RESPECTIVELY. N/A MEANS THAT THE SENSOR MODELS WERE NOT FULLY ACQUIRED AGAINST AT LEAST ONE COLOR.

	d_T			d_I		
Distance [mm]	MEAN	STD	E_{max}	MEAN	STD	E_{max}
85.4	85.9	1.3	4.6	N/A	N/A	N/A
75.4	75.8	1.3	3.6	N/A	N/A	N/A
65.4	64.9	1.3	2.6	N/A	N/A	N/A
55.4	55.0	1.4	3.4	N/A	N/A	N/A
45.4	45.2	1.1	3.4	N/A	N/A	N/A
35.4	35.1	1.2	3.4	35.9	2.0	6.8
25.4	29.2	1.9	7.6	26.7	1.6	5.0
15.4	16.6	1.5	4.6	14.7	1.3	2.7
5.4	9.1	1.4	8.6	5.7	0.3	1.2

I as b. After moving the hand to 85.4 mm, we repeated the measurements and one measurement step reduction in the distance. The distance from the rubber surface to the sheet on each step (e.g., 80 mm) was confirmed using a ruler with 1 mm graduations, which means that the error of each ground-truth distance should be ±0.1 mm.

Fig. 7 and Table II show the distance measurement results. At the distances in Stage 3 described in §II-B (i.e., 35.4, 25.4, 15.4, and 5.4 mm), the distance output d_I was generated from the intensity sensor, as expected. At all of these distances, except for 35.4 mm, d_I outperformed the ToF sensor output d_T in terms of the error of the mean and the standard deviation. Fig. 8 describes the intensity sensor output with the offset ($I - b$) obtained in this experiment. The sheets, except for the black sheet, showed similar properties, indicating that they had similar reflectance of the infrared light used by the intensity sensor. By contrast, the black sheet showed significantly different reflectance from the other sheets. For instance, the intensity value against pink was approximately 10 times as large as the value against black, resulting in the same ratio between the object-dependent parameters (a) of the two sheets. The difference between these intensity values was too big such that we had difficulty in using these values

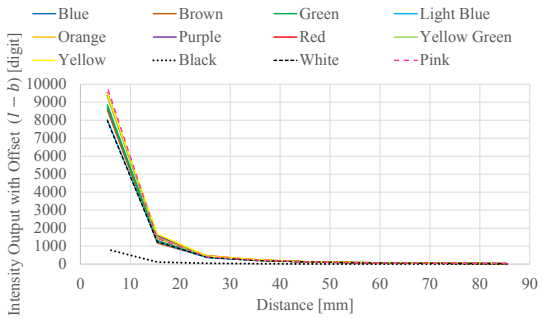

Fig. 8. Intensity sensor output with offset ($I - b$) against the colored sheets shown in Fig. 6. The output against pink (broken pink line) was approximately 10 times as large as the output against black (dotted black line). Thus, we had difficulty in using them in the same manner (e.g., using the same threshold for touch detection).

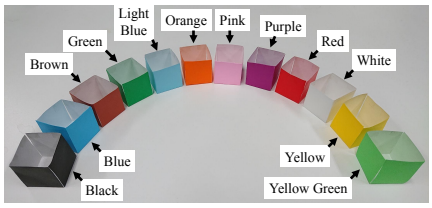

Fig. 9. Paper boxes used as compliant objects in §IV-B. These boxes were made from sheets of folding paper, had wall thicknesses of 0.07 mm, and measured 35 mm × 35 mm × 35 mm.

in the same manner (e.g., using the same threshold for touch detection). On the contrary, our module generated almost the same d_{I} against both the pink and black sheets, showing that our module had little dependence on reflectance, and d_{I} outperformed the intensity sensor output.

B. Picking Up Compliant Objects

We conducted five picking-up trials using our precise grasping system against 12 compliant colored boxes (Fig. 9). Their compliance came from the thinness of their paper walls (i.e., 0.07 mm). Fig. 10 shows a sequence of the experiments in this subsection. In Fig. 10c, we checked if the robot grasped the object gently enough not to squeeze it, and in Fig. 10d, we checked if the robot grasped the object firmly enough to lift it up. The following cases were tested for comparison:

- picking up only with the intensity sensors against the black and pink boxes, and
- grasping with pressure sensors against the red box.

In the former, our robot hand stopped its fingers when every intensity output with the offset fell below the threshold uniquely defined for each sensor (i.e., 336 for the left fingertip and 840 for the right fingertip). In the latter, we used the Willow Garage PR2 robot with its pressure sensor fingertips. We utilized the standard PR2 gripper sensor controller with the same thresholds as in the previous study [6] (i.e., 0.05 N for the high-passed pressure readings and 0.4 N for the unfiltered pressure).

Tables III and IV show the results of the task involving the picking up of compliant objects. As described in Table III, the deformations by our precise grasping system were smaller than those by the other methods. Table IV presents that our precise grasping was gentle and firm against all box colors. By contrast, the results of picking up only with the intensity sensors differed by color.

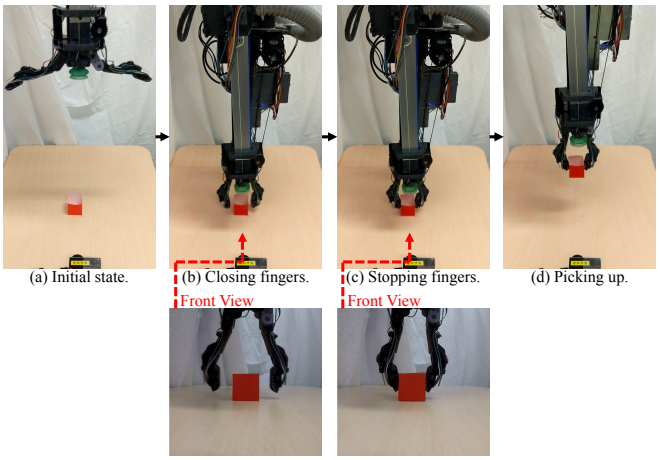

Fig. 10. Sequence of picking up the compliant objects: (a) the offset parameters b were acquired, (b) the fingers were closing, (c) the fingers were stopped by our precise grasping system, and (d) the robot executed the picking-up motion to check if the object was firmly grasped.

TABLE III
OBJECT DEFORMATIONS CAUSED BY THE GRASPING MOTIONS. WE SELECTED PICTURES OF THE LEAST AND MOST DEFORMED OBJECTS IN ALL TRIALS OF EACH METHOD. THE DEFORMATIONS BY OUR PRECISE GRASPING SYSTEM WERE SMALLER COMPARED TO THOSE BY THE OTHER METHODS.

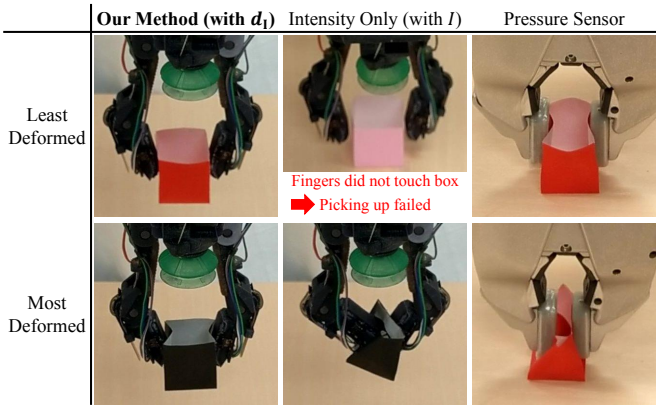

TABLE IV
CRITICAL FAILURE RATES OF PICKING UP THE COMPLIANT OBJECTS. "CRUSHING THE BOX" IS THE CASE IN WHICH ONE WALL OF THE BOX TOUCHES THE OPPOSED WALL. "DROPPING THE BOX" IS THE CASE IN WHICH THE BOX DROPS BEFORE IT IS LIFTED BY 110 mm. N/A EXISTS BECAUSE WE FOUND A LARGE DEFORMATION IN ALL TRIALS WITH THE PRESSURE SENSORS AND SKIPPED LIFTING. THE TRIALS WITH OUR METHOD HAD NO CRITICAL FAILURES. PICKING UP ONLY WITH THE INTENSITY SENSORS ALWAYS CRUSHED THE BLACK BOX AND MOSTLY DROPPED THE PINK BOX. CRUSHING THE BOX WAS NOT RARE WHEN THE PRESSURE SENSORS WERE USED.

	Our Method	Intensity Only	Pressure Sensor
Crushing the box	**0/60**	5/10	2/5
Dropping the box	**0/60**	4/10	N/A

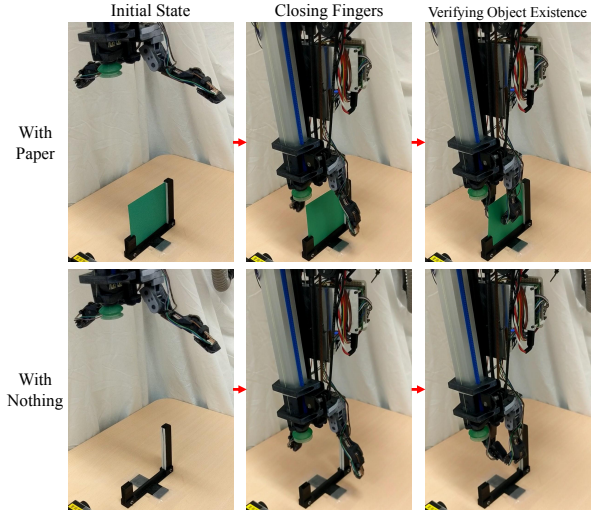

Fig. 11. Sequence of ultra-thin object grasping. Our grasp verification system tried to distinguish the upper case ("With Paper") from the lower case ("With Nothing"). In the upper case, one sheet (Fig. 6) was inserted into the slit of the jig on the table. The offset parameters (b) were acquired at the initial state. The object-dependent parameters (a) were acquired while the fingers were closed. These parameters were used to verify the sheet existence between the fingers.

C. Verification of Ultra-thin Object Grasping

Fig. 11 shows a sequence of the experiments in this subsection. We repeated this sequence for five times per one colored sheet against the 12 colored sheets (Fig. 6). We prepared a jig that kept a sheet vertical on the table. The object-dependent parameters a were acquired while the fingers were grasping that sheet. After grasping, the parameters were used to verify the sheet existence between the fingers. We also executed this sequence when no sheet was inserted to check whether the robot can detect that nothing exists between the fingers.

Fig. 12 shows the object-dependent parameters a acquired in the experiments. When a sheet of paper existed between the fingers, our system could mostly detect it because the parameters were mostly in the range of our grasp verification ($10000\,\mathrm{digit}\cdot\mathrm{mm}^2 \leq a \leq 2000000\,\mathrm{digit}\cdot\mathrm{mm}^2$). The only exception was one trial against the black sheet. When nothing existed between the fingers, our system could detect that because the parameters were zero. Zero was not entirely desirable because this value means failure in the sensor model acquisition. This value is attributable to the intensity sensor output I against a fingertip being too different from I against the object. This may show that one limitation of our sensor model acquisition is failure against objects with similar properties to the fingertip (e.g., a transparent layer is on an opaque layer).

D. Picking Up and Placing a Paper with Disturbances

Fig. 13 shows the sequence of picking up and placing a paper with disturbances by a person. In this experiment, loose leaves with $0.10\,\mathrm{mm}$ thickness were used. The robot hand slid the paper on the table, grasped the protruded part with three fingers, and placed the paper in the pressure clip file.

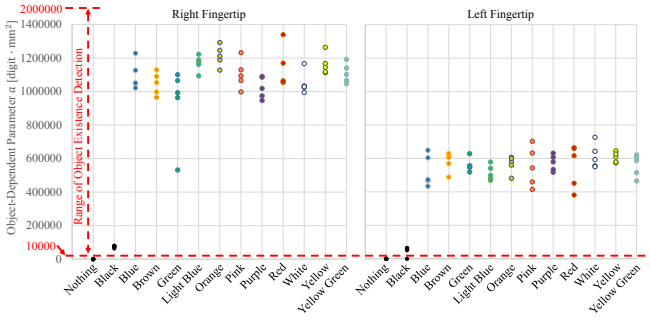

Fig. 12. Object-dependent parameters a output from our sensor modules in ultra-thin object grasping. Each dot denotes one parameter a acquired in one grasping trial. Two parameters were acquired in a grasping trial (by the left and right fingertips); hence, the graph has 130 dots. When a sheet of paper existed between the fingers, our system could mostly sense it because the parameters were mostly in the range of our grasp verification. The only exception was one trial against the black sheet. By contrast, the parameters were zero and out of the range when nothing existed between the fingers.

Although this hand can suction, suctioning was not used to avoid creasing the paper. We applied precise grasping with verification in Figs. 13c and g. If no object was detected (Fig. 13g), the robot considered that the paper was grabbed by the person and went back to the visual recognition state. The precise grasping was also used in Fig. 13j. Fig. 13i presents another usage of the precise distance output d_I. The values greatly changed (i.e., became big in this experiment) when the paper was grabbed by the person because these values were adjusted to the paper. This was used to detect grabbing. The robot then slightly opened its fingers to make the insertion easy. When the paper was inserted again, the values went back to the previous level, and the robot could detect it to perform grasping again.

V. CONCLUSION

This study proposes a method of acquiring parameters in models of optical reflection intensity sensors on a robot hand using optical ToF sensors while that hand is grasping an object. Although close-range approximate proximity sensors, such as intensity sensors, can sense a close range, they strongly depend on the object properties, and their maximum measurable distances are short. By contrast, long-range distance sensors, such as ToF sensors, have little dependence on the object properties and can measure a long distance, but cannot measure a close range precisely. Our goal herein was to acquire proximity sensors that have little dependence on the object properties and that can sense a wide range. To accomplish this, we made proximity sensor modules with intensity and ToF sensors. Simple fusion of the two sensor types remains dependent on the object properties at the close range. Hence, we used an intensity sensor model that explicitly includes an object-dependent parameter. This parameter was acquired when a sensed object was in the overlapping measurable range of the two sensor types. Subsequently, a precise distance value was generated from the intensity sensor output using the acquired model. We utilized the precise distance value for the robot to pick up compliant objects without damaging them by squeezing. We

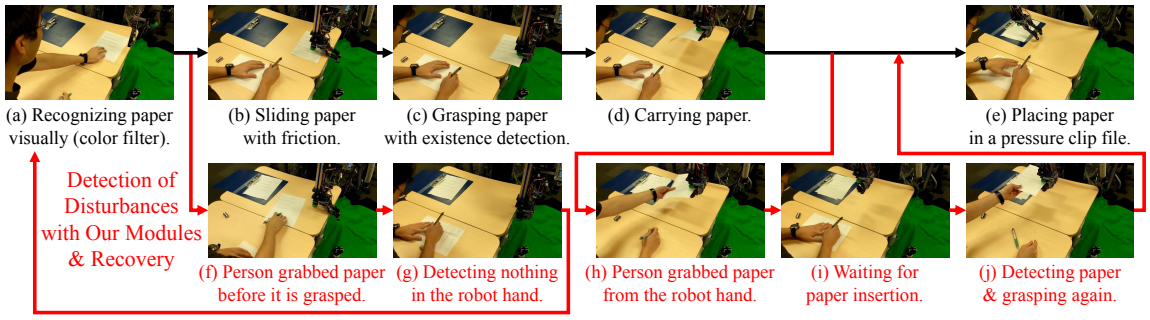

Fig. 13. Sequence of picking up and placing the paper with disturbances. Loose leaves with $0.10\,\mathrm{mm}$ thickness were used.

also used the object-dependent parameter to verify whether an ultra-thin object (e.g., a sheet of paper) exists between the fingers.

Using 12 colored sheets of paper, we validated that the distance output generated from the intensity sensor outperformed the ToF sensor at the close range ($\leq 25.4\,\mathrm{mm}$) in terms of the error of the mean and the standard deviation. We also experimentally confirmed that using the precise output suppressed the deformation of the 12 compliant colored boxes while they were being grasped compared to grasping only with the intensity sensors and grasping with the pressure sensors. The use of the acquired object-dependent parameters enabled the detection of whether a sheet existed between the fingers. Finally, we demonstrated picking up and placing the paper using our proposed methods, which can detect and recover from disturbances caused by a person.

References

[1] D. Balek and R. Kelley. Using gripper mounted infrared proximity sensors for robot feedback control. In *Proc. IEEE Int. Conf. Robot. Automat.*, Vol. 2, pp. 282–287, Mar. 1985.

[2] R. Wistort and J. R. Smith. Electric field servoing for robotic manipulation. In *Proc. IEEE/RSJ Int. Conf. Intell. Robots Syst.*, pp. 494–499, Sept. 2008.

[3] K. Hsiao, P. Nangeroni, M. Huber, A. Saxena, and A. Y. Ng. Reactive grasping using optical proximity sensors. In *Proc. IEEE Int. Conf. Robot. Automat.*, pp. 2098–2105, May 2009.

[4] J. Fujimoto, I. Mizuuchi, Y. Sodeyama, K. Yamamoto, N. Muramatsu, S. Ohta, T. Hirose, K. Hongo, K. Okada, and M. Inaba. Picking up dishes based on active groping with multisensory robot hand. In *Proc. 18th IEEE Int. Symp. Robot Human Interact. Commun.*, pp. 220–225, Sept. 2009.

[5] H. Hasegawa, Y. Mizoguchi, K. Tadakuma, A. Ming, M. Ishikawa, and M. Shimojo. Development of intelligent robot hand using proximity, contact and slip sensing. In *Proc. IEEE Int. Conf. Robot. Automat.*, pp. 777–784, May 2010.

[6] Liang-Ting Jiang and J. R. Smith. Seashell effect pretouch sensing for robotic grasping. In *Proc. IEEE Int. Conf. Robot. Automat.*, pp. 2851–2858, May 2012.

[7] S. Escaida Navarro, M. Schonert, B. Hein, and H. Wörn. 6d proximity servoing for preshaping and haptic exploration using capacitive tactile proximity sensors. In *Proc. IEEE/RSJ Int. Conf. Intell. Robots Syst.*, pp. 7–14, Sept. 2014.

[8] R. Patel, R. Cox, and N. Correll. Integrated proximity, contact and force sensing using elastomer-embedded commodity proximity sensors. *Auton. Robots*, Vol. 42, No. 7, pp. 1443–1458, Oct. 2018.

[9] K. Koyama, M. Shimojo, T. Senoo, and M. Ishikawa. High-speed high-precision proximity sensor for detection of tilt, distance, and contact. *IEEE Robot. Automat. Lett.*, Vol. 3, No. 4, pp. 3224–3231, Oct. 2018.

[10] S. Hasegawa, K. Wada, K. Okada, and M. Inaba. Detecting and picking of folded objects with a multiple sensor integrated robot hand. In *Proc. IEEE/RSJ Int. Conf. Intell. Robots Syst.*, pp. 1138–1145, Oct. 2018.

[11] K. Sasaki, K. Koyama, A. Ming, M. Shimojo, R. Plateaux, and J. Choley. Robotic grasping using proximity sensors for detecting both target object and support surface. In *Proc. IEEE/RSJ Int. Conf. Intell. Robots Syst.*, pp. 2925–2932, Oct. 2018.

[12] P. E. Lancaster, J. R. Smith, and S. S. Srinivasa. Improved proximity, contact, and force sensing via optimization of elastomer-air interface geometry. In *Proc. Int. Conf. Robot. Automat.*, pp. 3797–3803, May 2019.

[13] N. Yamaguchi, S. Hasegawa, M. Murooka, K. Okada, and M. Inaba. Selective grasp in occluded space by all-around proximity perceptible finger. *Robot. Auton. Syst.*, Vol. 127, p. 103464, 2020.

[14] J. Konstantinova, A. Stilli, A. Faragasso, and K. Althoefer. Fingertip proximity sensor with realtime visual-based calibration. In *Proc. IEEE/RSJ Int. Conf. Intell. Robots Syst.*, pp. 170–175, Oct. 2016.

[15] C. Bersch, B. Pitzer, and S. Kammel. Bimanual robotic cloth manipulation for laundry folding. In *Proc. IEEE/RSJ Int. Conf. Intell. Robots Syst.*, pp. 1413–1419, Sept. 2011.

[16] J. Kwiatkowski, D. Cockburn, and V. Duchaine. Grasp stability assessment through the fusion of proprioception and tactile signals using convolutional neural networks. In *Proc. IEEE/RSJ Int. Conf. Intell. Robots Syst.*, pp. 286–292, Sept. 2017.

[17] F. R. Hogan, M. Bauza, O. Canal, E. Donlon, and A. Rodriguez. Tactile regrasp: Grasp adjustments via simulated tactile transformations. In *Proc. IEEE/RSJ Int. Conf. Intell. Robots Syst.*, pp. 2963–2970, Oct. 2018.

[18] J. Xu, A. Bhardwaj, G. Sun, T. Aykut, N. Alt, M. Karimi, and E. Steinbach. Learning-based modular task-oriented grasp stability assessment. In *Proc. IEEE/RSJ Int. Conf. Intell. Robots Syst.*, pp. 3468–3475, Oct. 2018.

[19] R. Calandra, A. Owens, D. Jayaraman, J. Lin, W. Yuan, J. Malik, E. H. Adelson, and S. Levine. More than a feeling: Learning to grasp and regrasp using vision and touch. *IEEE Robot. Automat. Lett.*, Vol. 3, No. 4, pp. 3300–3307, Oct. 2018.

[20] Vishay, Malvern, Pennsylvania. Fully Integrated Proximity and Ambient Light Sensor with Infrared Emitter, I^2C Interface, and Interrupt Function. (2019). Accessed: May 11, 2020. [Online]. Available: `https://www.vishay.com/docs/84274/vcnl4040.pdf`.

[21] Pololu, Las Vegas, Nevada. Pololu - VL53L0X Time-of-Flight Distance Sensor Carrier with Voltage Regulator, 200cm Max. (2016). Accessed: Feb. 18, 2020. [Online]. Available: `https://www.pololu.com/product/2490`.

[22] STMicroelectronics, Geneva, Switzerland. World's smallest Time-of-Flight ranging and gesture detection sensor. (2018). Accessed: Feb. 18, 2020. [Online]. Available: `https://www.st.com/resource/en/datasheet/vl53l0x.pdf`.

[23] STMicroelectronics, Geneva, Switzerland. VL53L1X_DS.fm. (2018). Accessed: Feb. 18, 2020. [Online]. Available: `https://www.st.com/resource/en/datasheet/vl53l1x.pdf`.

[24] STMicroelectronics, Geneva, Switzerland. Proximity and ambient light sensing (ALS) module. (2016). Accessed: Feb. 18, 2020. [Online]. Available: `https://www.st.com/resource/en/datasheet/vl6180x.pdf`.

[25] R. Ma and A. Dollar. Yale openhand project: Optimizing open-source hand designs for ease of fabrication and adoption. *IEEE Robot. Automat. Mag.*, Vol. 24, No. 1, pp. 32–40, 2017.

[26] Y. Suzuki and T. Kitamura. Pci method: A novel fabrication method of soft mechanisms utilizing cure inhibition of addition reaction silicone. In *Proc. 2nd IEEE Int. Conf. Soft Robot.*, pp. 483–490, Apr. 2019.